

Ground-Based Solar Absorption FTIR Spectroscopy: Characterization of Retrievals and First Results from a Novel Optical Design Instrument at a New NDACC Complementary Station

A. WIACEK, J. R. TAYLOR, K. STRONG, R. SAARI, AND T. E. KERZENMACHER

Department of Physics, University of Toronto, Toronto, Ontario, Canada

N. B. JONES AND D. W. T. GRIFFITH

Department of Chemistry, University of Wollongong, Wollongong, New South Wales, Australia

(Manuscript received 13 October 2005, in final form 17 May 2006)

ABSTRACT

The authors describe the optical design of a high-resolution Fourier Transform Spectrometer (FTS), which serves as the primary instrument at the University of Toronto Atmospheric Observatory (TAO). The FTS is dedicated to ground-based infrared solar absorption atmospheric measurements from Toronto, Ontario, Canada. Instrument performance is discussed in terms of instrumental line shape (ILS) and phase error and modulation efficiency as a function of optical path difference. Typical measurement parameters are presented together with retrieval parameters used to derive total and partial column concentrations of ozone. Retrievals at TAO employ the optimal estimation method (OEM), and some impacts of the necessary a priori constraints are examined. In March 2004, after participating in a retrieval algorithm user intercomparison exercise, the TAO FTS was granted the status of a Complementary Observation Station within the international community of high-resolution FTS users in the Network for the Detection of Atmospheric Composition and Change (NDACC). During this exercise, average differences between total columns retrieved from the same spectra by different users were below 2.1% for O₃, HCl, and N₂O in the blind phase, and below 1% in the open phase, when all retrieval constraints were identical. Finally, a 2.5-yr time series of monthly mean stratospheric ozone columns agrees within 3% with those retrieved from Optical Spectrograph and Infrared Imager System (OSIRIS) measurements on board the *Odin* satellite, which is within the errors of both measurement platforms.

1. Introduction

The University of Toronto Atmospheric Observatory (TAO) has been operational since October 2001 and fills a coverage gap in midlatitude Canada within the Network for the Detection of Stratospheric Change (NDSC) described by Kurylo and Zander (2000). In 2005, the NDSC was renamed the Network for the Detection of Atmospheric Composition and Change (NDACC) in order to better reflect the scope of its activities. Ground-based Fourier transform infrared (FTIR) spectra recorded at NDACC stations have been widely used to retrieve long-term time series of ozone

and ozone profiles (Pougatchev et al. 1995; Barret et al. 2002; Schneider et al. 2005a) and related chemical species (Zander et al. 1994; Rinsland et al. 2002b, 2003; Schneider et al. 2005b).

TAO was established to acquire high-quality long-term measurements of trace gases for the purpose of understanding chemical and dynamical processes in the atmosphere and to validate models and satellite measurements of atmospheric constituents. The geographic position of TAO (43.66°N, 79.40°W) makes it well suited for measurements of midlatitude stratospheric ozone, related species, and greenhouse gases, while its urban setting enables measurements of tropospheric pollutants. The primary instrument at TAO is a high-resolution Fourier Transform Spectrometer (FTS) manufactured by ABB Analytical Business PRU Québec (Canada). The FTS is complemented by a commercially available weather station (Vantage Pro Plus

Corresponding author address: Aldona Wiacek, University of Toronto, Department of Physics, 60 St. George Street, Toronto, ON M5S 1A7, Canada.
E-mail: aldona@atmosph.physics.utoronto.ca

manufactured by Davis Instruments Corp.) that records local meteorological variables, UV radiation, and solar irradiance; and (on a campaign basis) by a Differential Optical Absorption Spectrometer (DOAS) (Bassford et al. 2001, 2005); and a Sun Photo Spectrometer (SPS) (McElroy 1995). A Meteorological Service of Canada (MSC) Brewer spectrometer and a ground-level ozone monitor were installed in 2005.

In section 2 we present details of our new facility and instrument characterization results obtained with the LINEFIT algorithm described by Hase et al. (1999), and in section 3 we detail our implementation of a data analysis and error characterization technique based on the optimal estimation method (OEM) as formulated by Rodgers (1976, 1990, 2000). We also discuss the impacts of a priori information on ground-based OEM retrievals of partial columns and profiles, which were highlighted during the algorithm user intercomparison exercise performed in order to evaluate the TAO FTS. As a direct result of this exercise, the TAO FTS was granted the status of a Complementary Station in the NDACC in March 2004. Finally, in section 4 we compare a 2.5-yr time series of ozone with measurements made by the Optical Spectrograph and Infrared Imager System (OSIRIS) instrument (von Savigny et al. 2003; Llewellyn et al. 2004) on board the *Odin* satellite (Murtagh et al. 2002).

2. Measurement technique

The FTS and its dedicated suntracker are located 174 m above sea level in downtown Toronto, Ontario, Canada. The altitude–azimuth suntracker (manufactured by AIM Controls Inc.) is housed in an electronically controlled weatherproof enclosure and provides continuous active solar tracking throughout the day. Figure 1 shows a schematic of the FTS and suntracker installation. To characterize the FTS instrument line shape (ILS) a dedicated blackbody (IR-563/301 manufactured by Infrared Systems Development Corp.) has also been installed at TAO and is coupled to the FTS through the same optics as the suntracker plus one additional removable 45° mirror (Fig. 1).

FTIR solar absorption spectra are recorded under clear-sky conditions, allowing for approximately 80 observation days per year in the first three years of operation. The temporal coverage of the dataset is more sparse in the winter months due to decreased daylight hours and increased cloud cover.

a. FTS design, configuration, and measurement parameters

The TAO FTS is manufactured by ABB Analytical Business PRU Québec. The DA8 model is a modified

Michelson interferometer (Fig. 2) with a maximum optical path difference of 250 cm, providing a maximum apodized resolution of 0.004 cm^{-1} . Until recently, a dynamic alignment approach was used whereby the position of the fixed mirror of the interferometer was adjusted to compensate for the deviations from alignment of the moving mirror; thus, the fixed mirror was not truly fixed. In the new design, the fixed mirror is permanently mounted and an adjustable flat mirror that folds the beam is added to the moving mirror arm of the interferometer (Fig. 2). It is this folding mirror that now provides dynamic alignment and compensates for any wobble of the moving mirror. At the same time, the dynamic alignment circuitry and actuation are kept stationary at the folding mirror. This arrangement results in a fixed optical axis through the beamsplitter (and a fixed focal point on the detector) as well as more stable modulation efficiency, which leads to an improved instrumental line shape and stability. The TAO FTS represents the first commercial implementation of this design on the 250-cm-OPD DA8, with a few other high-resolution DA8 spectrometers retrofitted with the dynamically aligned folding mirror since then.

The FTS is currently equipped with KBr and CaF₂ beamsplitters, and InSb and HgCdTe (MCT) detectors for coverage of the spectral range from 750 to 8500 cm^{-1} . The system is also equipped with six narrowband optical interference filters that are widely used in the NDACC Infrared Working Group (IRWG). Table 1 summarizes trace gases commonly measured with this filter set, both detectors and the KBr beamsplitter. This FTS configuration (operating under vacuum) is used during regular solar absorption measurements. Built-in globar and quartz halogen sources (Fig. 2) as well as an external collimated blackbody are used during instrument characterization.

Solar absorption measurements are semiautomated, involving an operator at start up and shut down to engage the suntracker, cool the detectors with liquid nitrogen, and initiate an automatic measurement sequence. All spectra are recorded without apodization, nominally using the settings summarized in Table 2.

b. FTS characterization

The alignment and performance of an FTS is characterized by its ILS (e.g., Park 1982; Goorvitch 2000). Accurate knowledge of the ILS is necessary in order to retrieve information on the vertical distribution of trace gases from FTIR spectra, which is contained in the spectroscopic absorption line shapes (Schneider et al. 2005a). Bernardo and Griffith (2005) showed that accurate knowledge of the ILS can reduce errors in the retrieved absorber amount by as much as 12%. For

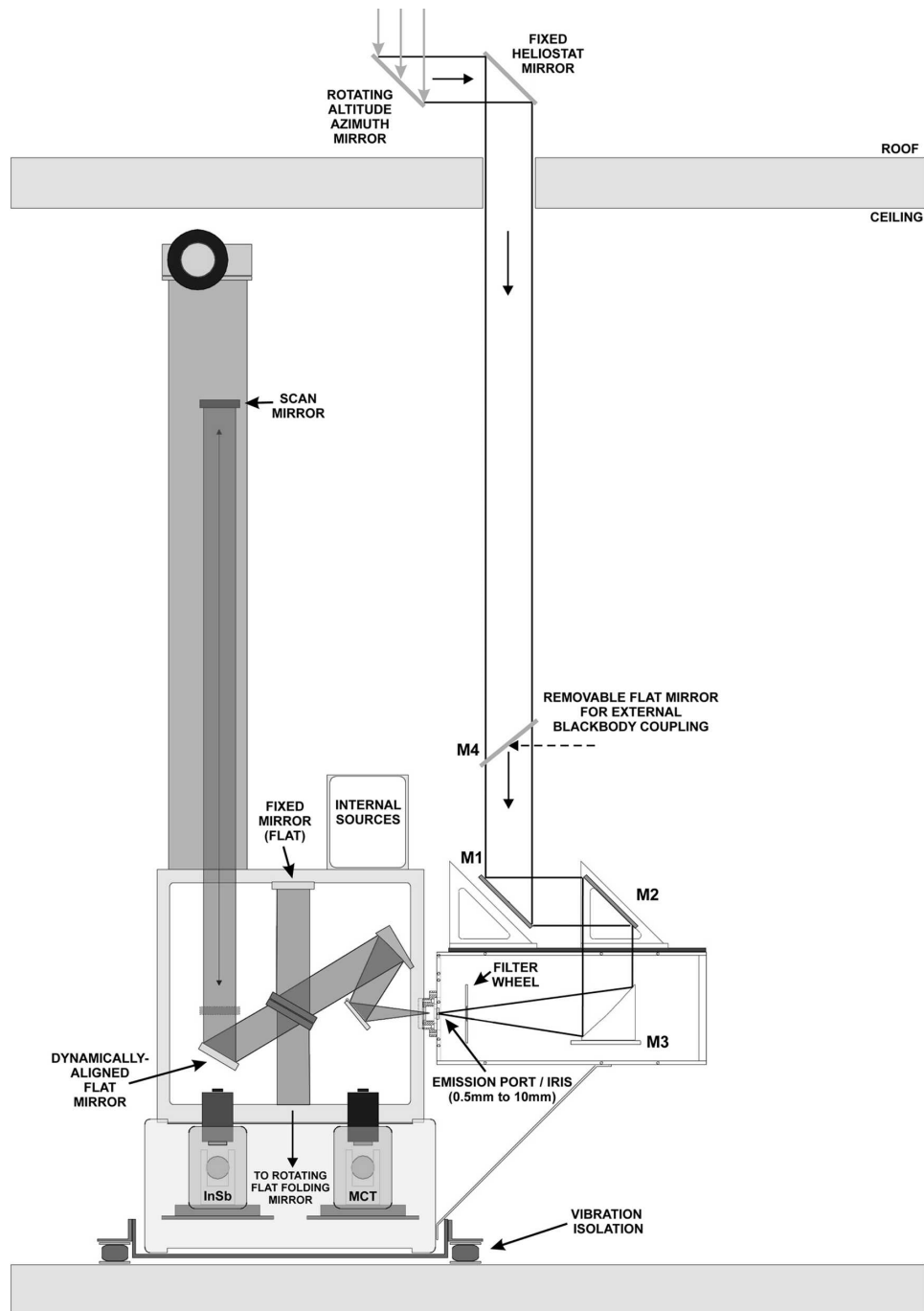


FIG. 1. FTS and suntracker installation at TAO (adapted from ABB Analytical Business PRU Québec facility schematics). The M1, M2, and M3 serve to couple the heliostat optics to the DA8 FTS. A removable 45° mirror (M4) couples the FTS to a blackbody for instrumental line shape testing.

these reasons the ILS of the TAO FTS is monitored on a regular basis by means of calibrated low-pressure N₂O and HBr gas cell measurements and the newly developed ILS retrieval algorithm described by Hase et al. (1999). We apply the latest version of that retrieval

software (LINEFIT version 9) to characterize the phase error and modulation efficiency of our instrument as a function of optical path difference (OPD) from high signal-to-noise-ratio (SNR) transmission spectra of N₂O and HBr absorption features. Unlike N₂O, HBr

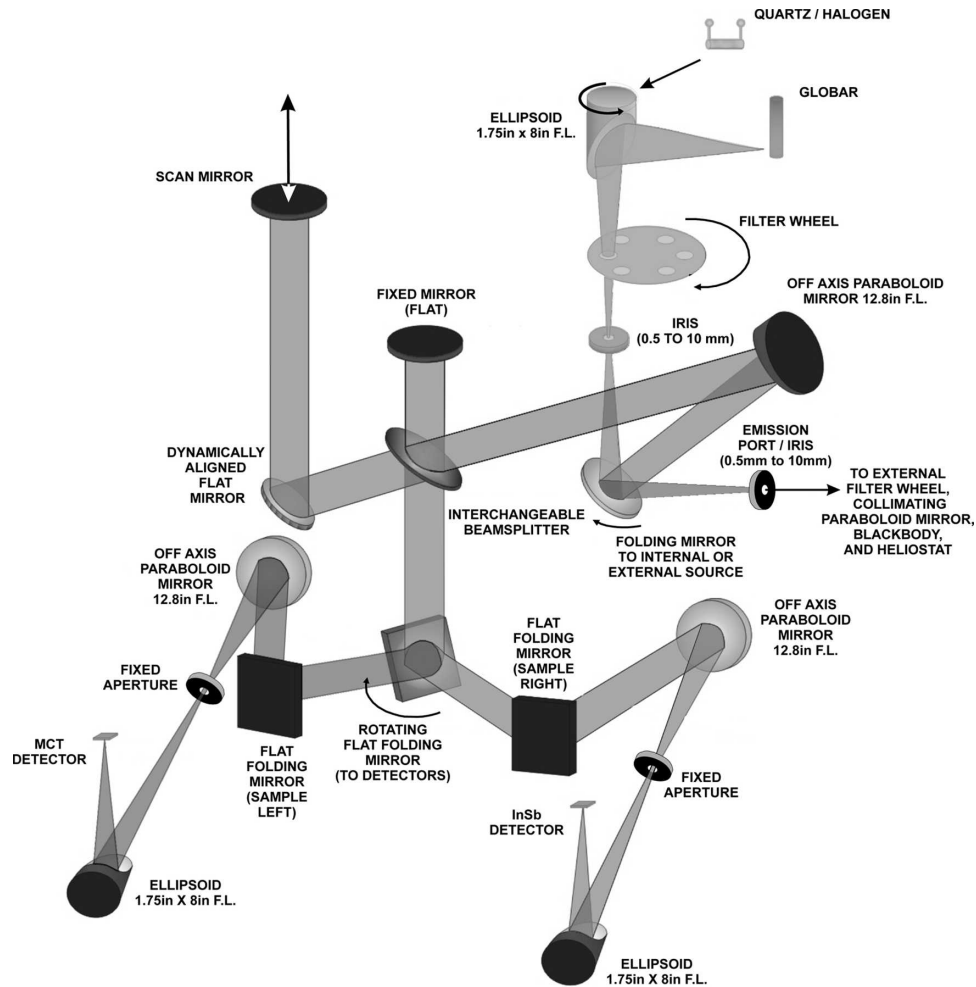


FIG. 2. The DA8 FTS is a modified Michelson design. A moving folding mirror selects between the emission port used for solar absorption measurements and blackbody line shape testing, and internal sources (shown in the faded portion at top right) used for some instrument alignment. (Adapted from ABB Analytical Business PRU Québec instrument schematics.)

cell measurements can additionally be used to determine the ILS of an FTS directly while solar absorption spectra are being recorded, since the atmosphere has no appreciable quantities of HBr (Coffey et al. 1998). For an ideally aligned FTS with perfect optics and an infinitesimal field of view (FOV) the phase error is zero

and the modulation efficiency is one at all path differences in the interferometer.

At TAO, low-pressure gas cell measurements can be made using a calibrated, 1050°C blackbody radiation source optically coupled to the emission port of the spectrometer, the internal globar source, or the sun

TABLE 1. Spectral coverage of the NDACC filter set.

NDACC filter	Wavenumber (cm ⁻¹)	Wavelength (μm)	10 standard NDACC targets (in bold in their typical retrieval regions at TAO)
1	4000–4300	2.3–2.5	HF , CO . . .
2	2900–3500	2.6–3.3	H₂O , C ₂ H ₂ , HCN . . .
3	2400–3100	3.3–4.1	O₃ , HCl , N₂O , CH₄ , NO₂ , C ₂ H ₆ , H ₂ O, CO ₂ . . .
4	2000–2700	3.9–5.0	CO, OCS, N ₂ . . .
5	1500–2200	4.7–6.3	CO, NO , COF ₂ . . .
6	750–1350	7.4–14	O ₃ , ClONO₂ , HNO₃ , N ₂ O, CH ₄ , C ₂ H ₂ , C ₂ H ₄ , CFCs . . .

TABLE 2. Measurement parameters used with the TAO FTS.

	Resolution (cm^{-1})	No. of scans co-added*	Full field of view (mrad)**	Detector
Filters 1–5	0.004	4	1.54	InSb
Filter 6	0.005	5	4.63	HgCdTe (MCT)

* Co-adding time is approximately 20 min in both cases to limit SZA changes.

** Defined as input aperture diameter divided by focal length of input optics (324 mm).

(Fig. 2). The gas cell is placed in the focused beam of radiation in the evacuated sample compartment (below the beamsplitter and immediately before the InSb detector) in order to limit cell temperature variations. Typically, a spectrum consisting of 50 co-added scans is recorded at maximum resolution (0.004 cm^{-1}) with all other measurement settings matching those used for TAO atmospheric observations. Transmission spectra are generated by taking the ratio of a full cell spectrum to an empty beam spectrum for the HBr cell and an empty cell spectrum for the N_2O cell, thus eliminating systematic features associated with water vapor absorption and detector baseline nonlinearity. Selected mi-

crowindows in the transmission spectra, each containing a single HBr or N_2O absorption feature, are simultaneously fitted with the LINEFIT algorithm; the modulation efficiency and phase error as a function of OPD are adjusted until the spectral fit residual is minimized. These experiments are performed every three to four months at TAO.

Recent (June 2005) fits of HBr transmission spectra and the corresponding retrieved ILS, modulation efficiency, and phase error are shown in Fig. 3 for six HBr cells filled to ~ 2 mbar in 2001 using one gas distribution manifold and used at six different NDACC stations (M. T. Coffey et al. 2001, personal communication). The 2-cm-long sealed glass cells with 2.5-cm-diameter fused sapphire windows were maintained at room temperature throughout the measurements. A thermocouple was placed inside the sample compartment to monitor the initial and final ambient temperature, and the mean of the two values was used in the LINEFIT retrievals, with the largest observed difference for any given spectrum being 0.9°C . The HBr spectra were recorded at 0.004 cm^{-1} resolution using the internal global source and co-adding 50 scans over a period of 4.5 h per spectrum. Background spectra consisted of 100 co-added scans. The root-mean-square (RMS) noise in the spectral fits is well below 1% and comparable to values

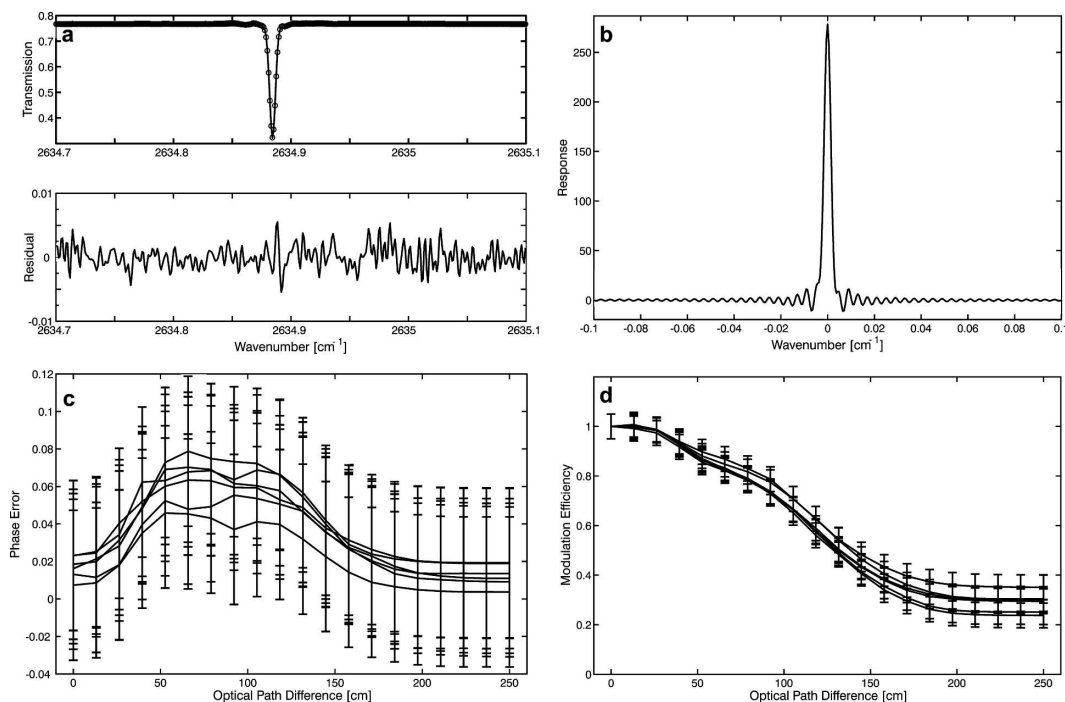


FIG. 3. (a) Observed (solid) and fitted (circles) HBr line (R4), with residual shown in the lower panel. (b) Sample ILS retrieved by LINEFIT. (c) Retrieved phase error from six different HBr cells. (d) Retrieved modulation efficiency from six different HBr cells. All measurements and ILS retrievals performed in June 2005.

reported by Hase et al. (1999). The phase error is well below 0.1 rad for all optical path differences in the FTS and results in the small asymmetry visible in the ILS. The modulation efficiency drops to approximately 30% at maximum OPD and implies a reduction in the theoretical resolution (0.004 cm^{-1}) and a possible misalignment of the instrument. Efforts to improve the alignment of the TAO FTS are ongoing, and we are presently investigating the full effect of using the LINEFIT ILS parameters on retrieved trace gas profiles and the information content of the measurements. Since a given atmospheric absorption feature will appear broader than it truly is, the retrieved profile for the corresponding gas will shift to lower altitudes, where the Lorentz broadening of spectral lines is greater. In general, the effects of an imperfect ILS become smaller for total column retrievals, which are less sensitive to the details of the absorption line shape (section 3), and are approximately proportional to the area under the absorption curve.

3. Data analysis

In ground-based Fourier transform infrared spectroscopy, information about the vertical distribution of atmospheric trace gases is derived from well-resolved Lorentz-broadened solar absorption line shapes. The observation geometry of ground-based measurements, the maximum achievable spectral resolution and measurement SNR limits the vertical resolution to at best 5–10 km [see, e.g., Pougatchev et al. (1995), Barret et al. (2002), or Schneider et al. (2005a) for a discussion of the vertical resolution of retrieved O_3 profiles]. Vertical resolution can be improved by combining multiple spectral features of varied absorption strength in one retrieval (Barret et al. 2002). The typical range of vertical sensitivity is taken to be approximately 45 km and can be increased by choosing absorption lines at lower wavenumbers, which have smaller (confounding) contributions from Doppler broadening (Schneider et al. 2005a).

a. Retrieval theory

The OEM is commonly employed in the underdetermined problem of deriving a vertical profile of an atmospheric trace gas from a ground-based solar absorption spectrum. This topic has been described in the literature (Rodgers 1976, 1990, 2000), and in this paper we only recount basic formulas relevant to our work.

In OEM the a priori knowledge, \mathbf{x}_a , of the n -dimensional state vector \mathbf{x} (e.g., the vertical profile of the trace gas of interest) is combined with the m -

dimensional measurement vector \mathbf{y} (e.g., spectral measurements related to the vertical profile by a nonlinear *forward model*) as a weighted mean. The weights are determined by the (matrix) covariance of the a priori profile, \mathbf{S}_a , and the (matrix) covariance of the random spectral measurement noise $\boldsymbol{\varepsilon}$, given the symbol \mathbf{S}_ε . If the forward model \mathbf{F} , including model parameters b , is linear in \mathbf{x} [i.e., $\mathbf{y} = \mathbf{F}(\mathbf{x}, b) + \boldsymbol{\varepsilon} = \mathbf{K}\mathbf{x} + \boldsymbol{\varepsilon}$], the optimal solution is given by

$$\hat{\mathbf{x}} = (\mathbf{S}_a^{-1} + \mathbf{K}^T \mathbf{S}_\varepsilon^{-1} \mathbf{K})^{-1} (\mathbf{S}_a^{-1} \mathbf{x}_a + \mathbf{K}^T \mathbf{S}_\varepsilon^{-1} \mathbf{y}), \quad (1)$$

where \mathbf{K} is the weighting function matrix. Equation (1), which is analogous in form to the linear combination of two scalars with known variances, can also be written as

$$\hat{\mathbf{x}} = \mathbf{x}_a + \mathbf{G}\mathbf{K}(\mathbf{x} - \mathbf{x}_a) = \mathbf{x}_a + \mathbf{A}(\mathbf{x} - \mathbf{x}_a), \quad (2)$$

where the *gain matrix* \mathbf{G} is given by

$$\mathbf{G} = (\mathbf{S}_a^{-1} + \mathbf{K}^T \mathbf{S}_\varepsilon^{-1} \mathbf{K})^{-1} \mathbf{K}^T \mathbf{S}_\varepsilon^{-1}, \quad (3)$$

and the *averaging kernel matrix* \mathbf{A} is defined as the product of \mathbf{G} and \mathbf{K} . The rows of the $n \times m$ \mathbf{G} matrix are commonly referred to as the *contribution functions* and represent the sensitivity of the retrieved state to the measurements. The rows of the $m \times n$ \mathbf{K} matrix are commonly referred to as *weighting functions* and represent the sensitivity of the forward model to the true state. By definition, the rows of the $n \times n$ \mathbf{A} matrix give the sensitivity of the retrieved state to the true state:

$$\mathbf{A} = \mathbf{G}\mathbf{K} = \frac{\partial \hat{\mathbf{x}}}{\partial \mathbf{y}} \frac{\partial \mathbf{F}(\mathbf{x})}{\partial \mathbf{x}} = \frac{\partial \hat{\mathbf{x}}}{\partial \mathbf{x}}. \quad (4)$$

For a measurement system that resolves each element of the retrieved state vector with perfect sensitivity, \mathbf{A} equals the identity matrix. The n th row of \mathbf{A} then corresponds to a delta function response to the n th element of the retrieved state vector. The n th column of \mathbf{A} is the impulse response to a perturbation in the n th element of the true state vector. In ground-based FTIR measurements the diagonal elements of \mathbf{A} are not unity (representing imperfect sensitivity to the true state at all heights) and off-diagonal elements are present (representing the inability to independently resolve all elements of the retrieved state vector).

The above results are strictly valid where the measurement and state vectors are linearly related and where the measurement and a priori error covariance statistics are Gaussian. More commonly the forward model \mathbf{K} is only a linearization about a reference state, here taken to be the a priori state ($\mathbf{K} = \partial \mathbf{F} / \partial \mathbf{x}$ is a matrix of derivatives evaluated at the reference state). In this

TABLE 3. Average degrees of freedom for signal in total and partial column retrievals in 2004.

	CH ₄	N ₂ O	O ₃	HCl	HF	NO	NO ₂
0–100 km	3.62	4.12	2.01	2.88	2.45	1.22	1.10
0–15 km	2.42	2.71	0.10	0.24	0.18	0.02	0.03
15–50 km	1.21	1.41	1.91	2.62	2.27	1.09	1.07

case the optimal solution is obtained using Newtonian iteration and is given by

$$\mathbf{x}_{i+1} = \mathbf{x}_a + (\mathbf{S}_a^{-1} + \mathbf{K}_i^T \mathbf{S}_\epsilon^{-1} \mathbf{K}_i)^{-1} \mathbf{K}_i^T \mathbf{S}_\epsilon^{-1} [(\mathbf{y} - \mathbf{y}_i) - \mathbf{K}_i(\mathbf{x}_a - \mathbf{x}_i)], \quad (5)$$

where \mathbf{K}_i is taken to mean “ \mathbf{K} evaluated at \mathbf{x}_i ” and $\mathbf{y}_i = \mathbf{F}(\mathbf{x}_i)$.

The number of state vector elements that are independently resolved is calculated by taking the trace of \mathbf{A} and is referred to as the *degrees of freedom for signal* (Rodgers 2000) in the measurement

$$d_s = \text{tr}(\mathbf{A}). \quad (6)$$

By taking the trace of \mathbf{A} over a certain vertical range of the atmosphere, we determine the number of independently resolved pieces of information present in the partial column derived from this region. Table 3 shows typical d_s values for a set of seven species retrieved from TAO spectra in microwindows detailed in Table 4.

b. Retrieval algorithm

The above OEM formulation of Rodgers (1976, 1990, 2000) is implemented semiempirically in the SFIT-2 algorithm (version 3.81 and 3.82 $\beta 3$ were used in this study) developed at the National Aeronautics and Space Administration (NASA) Langley Research Center and the National Institute of Water and Atmospheric Research (NIWA; Pougatchev et al. 1995; Connor et al. 1996; Rinsland et al. 1998). It has been successfully compared to another OEM retrieval algorithm by Hase et al. (2004). The characterization of vertical information contained in high-resolution FTIR spectra is of ongoing interest to the NDACC; the more sophisticated vertical profile and partial column data products clearly have more uses in basic research and satellite validation applications than the more limited vertical columns.

The first step in our retrieval is to calculate a model atmosphere using the ray tracing program *fscatm* documented extensively by Gallery et al. (1983). Recent improvements to the code are described by Meier et al. (2004). The *fscatm* program converts pressure, tem-

TABLE 4. Microwindows and interfering species used in operational TAO retrievals, which typically also retrieve the background slope and curvature, wavenumber shift, and simple phase forward model parameters.

Target gas	Microwindow (cm ⁻¹)	Interfering species	Mean SNR
O ₃	3045.0975–3045.3500	H ₂ O, CH ₄	350
CH ₄	2650.8500–2651.2500	HDO	650
	2666.9500–2667.3500		
	2673.9000–2674.4100		
N ₂ O	2481.3000–2482.6000	CO ₂ , CH ₄ , O ₃	
NO	1899.8800–1900.1500	CO ₂ , H ₂ O	250
NO ₂	2914.5900–2914.7070	CH ₄ , H ₂ O	1000
HCl	2925.8000–2926.0000	CH ₄ , NO ₂ , O ₃	850
HF	4038.7700–4039.1300	H ₂ O, HDO, CH ₄	350

perature, and volume mixing ratio (VMR) profiles specified at 63 layer boundaries to density-weighted effective pressure, temperature, and VMR profiles within the 38 layers that form the vertical retrieval grid used at TAO. The program also calculates airmass factors for each layer, given pressure and temperature profiles from the National Centers for Environmental Prediction (NCEP) reanalyses available through the NASA Goddard Space Flight Center automailer (http://hyperion.gsfc.nasa.gov/Data_services/automailer/index.html). We examined the effect of using in situ temperatures and pressures from the weather station instead of the lowest NCEP profile values on retrievals of CO and HCl; retrieved total column differences were negligible for both species, while retrieved VMR profile differences were well below 0.5% and 0.01%, respectively, at all heights.

VMR profiles of the 10 NDACC target atmospheric trace gases (Fig. 4) are constructed from a combination of 123 Halogen Occultation Experiment (HALOE) version 19 solar sunset occultation profiles between 1991 and 2004 and between approximately 15 and 60 km and within $\pm 5^\circ$ in latitude and longitude of TAO (Russell et al. 1993) for HCl, HF, O₃, NO, and NO₂; midlatitude daytime 2001 Michelson Interferometer for Passive Atmospheric Sounding (MIPAS; Carli et al. 2004) reference a priori profiles (<http://www.atm.ox.ac.uk/group/mipas/species>) for N₂O, CH₄, H₂O, and HNO₃; and Jet Propulsion Laboratory (JPL) MkIV FTS balloon flight data (<http://mark4sun.jpl.nasa.gov/balloon.html>) for ClONO₂. A priori profiles for trace gases not routinely retrieved and minor interfering species are constructed from a combination of these sources, model outputs, and other refereed literature.

During the iterative retrieval, the model atmosphere is used in each iteration to calculate the infrared absorption spectrum of the target gas (plus any signifi-

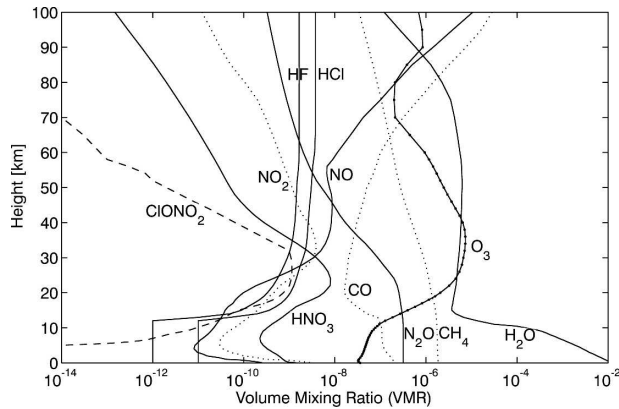


FIG. 4. A priori profiles of volume mixing ratios used in TAO retrievals for the 10 NDSC target gases and CO. Profiles are based on a combination of sources discussed in the text.

cantly absorbing interfering species) in a small microwindow ($\sim 1 \text{ cm}^{-1}$ wide). Pressure- and temperature-dependent absorption line parameters are obtained from the high-resolution transmission molecular absorption (HITRAN) 2004 spectral database (Rothman et al. 2005), except in section 3c, where an older version of the database was used (Rothman et al. 2003). The absorption cross sections are calculated assuming a Voigt line shape on a grid of 0.0005 cm^{-1} .

The instrument forward model includes a wavenumber scale multiplier, resolution, field of view, any apodization imposed digitally during the recording of the interferogram (none at TAO), as well as empirical apodization and phase error parameters. The two empirical parameters can be set to 0, or to a set of tabulated values (e.g., those provided by LINEFIT), or a polynomial of user-specified order n . The LINEFIT results (Fig. 3) were not used in this work; however, their incorporation into retrievals is presently under investigation at TAO.

The simulated spectrum can include absorption features originating in the atmosphere of the sun as previously described in detail by Rinsland et al. (1998). (The improved solar database available with SFIT-2 version 3.90 and higher was not used.) Continuous broadband extinction features due to aerosols in the earth's atmosphere are modeled by a background slope and curvature parameter. Commonly, we retrieve only the scaling factors applied to the a priori profiles of the interfering species, while full vertical profiles are only retrieved for the target gas in a given microwindow. Thus, the retrieved state vector \mathbf{x} consists of 38 target gas profile elements, usually a few scaling factors for profiles of interfering gases, and a few retrieved forward model parameters such as wavenumber shift,

background slope, solar line shifts, and constant phase error.

Finally, the user must construct a measurement error covariance matrix \mathbf{S}_e and an a priori covariance matrix \mathbf{S}_a that will be used in the iterative retrieval scheme [Eq. (5)]. Here \mathbf{S}_e is constructed diagonal and all elements are set to the inverse of the square of the SNR (calculated as the maximum signal in the microwindow divided by the RMS noise in the microwindow for a previous retrieval). In neglecting off-diagonal elements we assume uncorrelated measurement errors in the spectral domain. The construction of \mathbf{S}_a is more challenging in that it requires knowledge of the *true* variability of the target trace gases from 0 to 100 km, most commonly unknown or only partially known. Typically a diagonal and uncorrelated \mathbf{S}_a is assumed, which has a stabilizing effect on the retrievals (Rodgers and Connor 2003). The magnitude of the diagonal elements is estimated from measurements where possible, for example, from the previously described HALOE climatology, and smoothly extended throughout the entire vertical extent of the retrieval grid. While we have calculated full covariance matrices between 15 and 60 km for the seven species measured by HALOE, their implementation into operational retrievals requires care (the matrices must be constructed positive definite over the full retrieval grid) and is the subject of current research at TAO and by, for example, Hase et al. (2004). Finally, we have also performed retrievals with prior covariances that allow for correlations between different height levels; we used covariances of Gaussian form, with typical correlation lengths of 4 km; however, the results of this separate study are beyond the scope of this paper and will be the subject of a future publication.

Together with the weighting function matrix, \mathbf{S}_e and \mathbf{S}_a determine the quantity and vertical distribution of the independent pieces of information in the retrieval [Eqs. (3), (4), and (6)], and typical values derived from our high-resolution FTIR spectra are shown in Table 3. Furthermore, the covariance matrices determine the error budget, as discussed in section 4 [Eq. (8)]. As such, the importance of their realistic estimation and impact on retrievals is widely recognized.

c. Retrieval algorithm user intercomparison

Side-by-side instrument and algorithm intercomparisons comprise a part of the NDACC instrument and site validation protocol (<http://www.ndsc.ncep.noaa.gov/organize/protocols/appendix4/>). Instrument side-by-side intercomparisons of retrieval results have been described by Paton Walsh et al. (1997), Goldman et al. (1999), Griffith et al. (2003), and Meier et al. (2005).

Since these studies included different retrieval algorithms (sometimes employing different retrieval techniques), they did not focus on details of differences due to different retrieval constraints. Hase et al. (2004) focus specifically on an intercomparison of two different software implementations of the OEM retrieval, and they describe results for matched and unmatched constraints. Our study differs in that we describe how the results obtained by different users can differ when the same retrieval algorithm is applied to the same set of spectra. This can be termed a *retrieval algorithm user intercomparison*; however, the root causes of any differences in retrieval results are, of course, the implicit and explicit constraints necessitated by the OEM approach.

In ideal circumstances a side-by-side instrument intercomparison is highly desirable, provided that instrument alignment and retrieval constraint differences can be accounted for. However, it was not possible to arrange for the traveling FTS that was used in past NDACC intercomparisons to be shipped to Toronto. A validation exercise was designed to demonstrate the retrieval capabilities of the Toronto group (and also the Bremen, Germany, candidate NDACC Complementary Observation Station, which will not be described in this paper) as follows. Toronto and Wollongong investigators exchanged a small set of quality-controlled spectra recorded at Toronto, Wollongong, and Lauder. The Wollongong spectra were also recorded using a 250-cm-OPD Bomem DA8 FTS previously described by Rinsland et al. (2001) and retrofitted with the design described in this work, while the Lauder spectra were recorded using a 257-cm-OPD Bruker 120M FTS previously described by Rinsland et al. (2002a). Although the spectra were recorded by three different instruments, each team analyzed all spectra using the SFIT-2 algorithm, retrieving O_3 , N_2O , and HCl from their own spectra and from the spectra of the other team. The analyses performed at Wollongong became the controls, with the Wollongong investigators refereeing the exercise. Corresponding to spectra from each site, a set of a priori profiles of VMR, temperature, and pressure was agreed upon and used by both teams; the retrieval microwindows and major interfering species were also prescribed in the blind phase of the intercomparison, and the spectral database used was that documented in Rothman et al. (2003). The a priori VMR profiles of the target gases (O_3 , N_2O , HCl) were allowed to vary at all heights in a full profile retrieval, whereas the a priori VMR profiles of the major interfering species (e.g., CO_2 , H_2O) were scaled by a single (retrieved) factor; S_e and S_a were left to the discretion of the investigators in the blind phase of the intercomparison, as were any

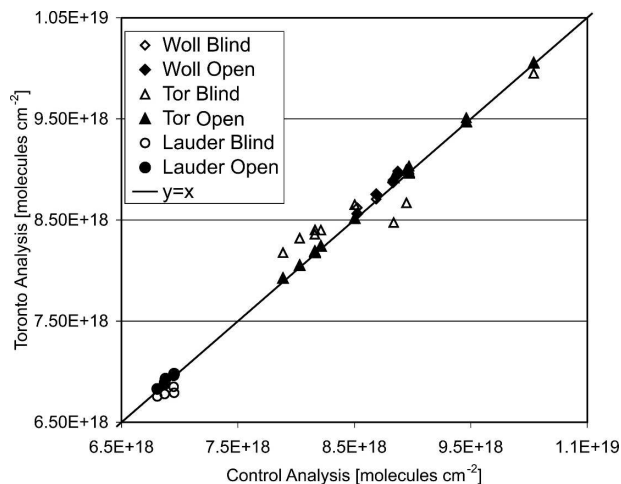


FIG. 5. Total columns of ozone (molec cm^{-2}) retrieved in the control analysis and in the Toronto analysis during both the blind and the open phase of the exercise.

other retrieved forward model parameters and minor interfering species. In the open phase of the intercomparison, all of the above were matched to the parameters used in the control analysis performed at Wollongong. For example, the Toronto spectra were analyzed using S_e of 440, 380, and 350 for O_3 , HCl , and N_2O in the blind phase, and 200, 200, and 150, respectively, in the open phase. Similarly, in the blind phase, Toronto spectra were analyzed using diagonal S_a matrices with 20% standard deviations at all heights for all three target gases, while in the open phase a 4-km correlation length was applied for O_3 retrievals, none was used in HCl retrievals, and a 3-km correlation length was again used in N_2O retrievals. Furthermore, the diagonal elements of S_a were not constant as a function of height for all three target gases in the open phase, where the standard deviations ranged between 0% and 100%. Finally, very similar constraint differences were present in the blind and open phase retrievals of O_3 , HCl , and N_2O from Wollongong and Lauder spectra.

The blind and open phase total column retrieval results for all analyzed spectra are shown in Figs. 5–7 for each of the target gases. The results of our intercomparison show that two different users analyzing the same spectra with the same auxiliary a priori information (VMR, pressure, and temperature profiles) but different a priori and measurement covariances, as described above, (some) different retrieved forward model parameters (e.g., transmission spectrum background slope and curvature fitting, wavenumber shift fitting), and (some) different minor interfering species (e.g., OCS) can expect average differences of 2.1% for O_3 , 1.6% for HCl , and 0.3% for N_2O . For comparison,

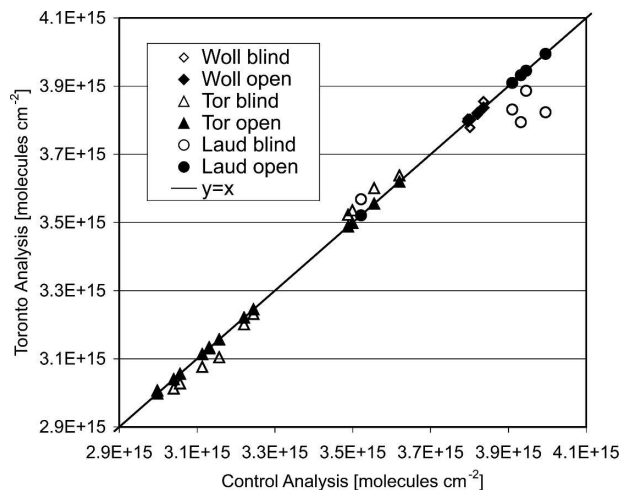
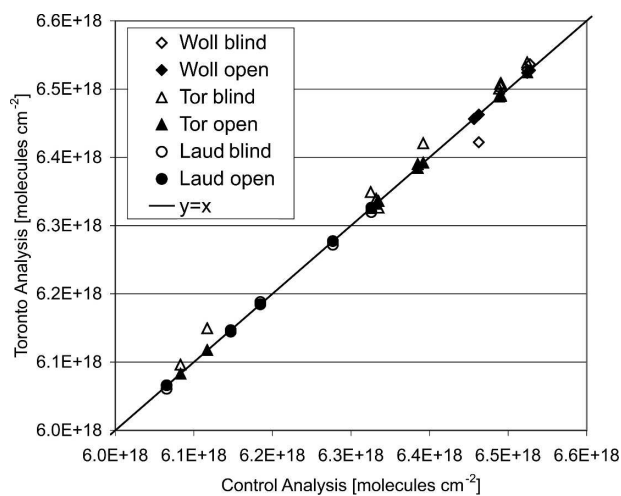


FIG. 6. Same as in Fig. 5, but for HCl.

Schneider et al. (2005b) summarize total column random errors due to solar zenith angle (SZA), temperature profile, measurement noise, and smoothing as 2.6% for O_3 , 2.2% for HCl, and 0.8% for N_2O . [A detailed discussion of error analysis in FTIR measurements is presented in Schneider et al. (2005a).] Only after controlling for all differences due to retrieval constraints, minor interfering species and retrieved forward model parameters do the average differences in the open phase of the intercomparison fall below 1% (0.83% for O_3 , 0.92% for HCl, and 0.05% for N_2O). The remaining differences are ascribed to small differences in the retrieval grid (38 layers at Toronto versus 36 layers at Wollongong), minor differences in the versions of the SFIT-2 software used, and the propagation of rounding errors to the retrieved solution. The effect of HCl retrieval parameters was studied in some detail

FIG. 7. Same as in Fig. 6, but for N_2O .

and differences in retrieved total column amounts of up to 5% were observed over a range of retrieval parameter values such as different a priori covariances of profile scaling factors for interfering species (N_2O , CH_4 , H_2O), the omission or inclusion of a minor interfering species (OCS), different values of the a priori wavenumber scale multiplier, and slightly different micro-window boundaries. While no strict generalizations to other species are practical or appropriate because of the nonlinear nature of the retrieval forward model, this number is representative of expected total column differences if the retrieval parameters that are used in the same software implementation of a retrieval algorithm are somewhat different.

Our total column differences below 1% are consistent with the findings of Meier et al. (2005), although our two studies are not precisely comparable since a nonlinear least squares fitting approach was used by Meier et al. to derive the total column amounts, as opposed to the OEM approach used here to derive the full profile first and later integrate it using the airmass profile as a weighting. However, our results support the general conclusions of Meier et al. (2005), which are that instrumental differences (for well-aligned spectrometers) are often smaller than systematic differences due to differences in the details in the analysis approach, which are in turn smaller than day-to-day variability of the observed gases. More precisely, our study also points to the importance of the consistency in the analysis approach (including all elements of the retrieved state vector and all constraining information) for the detection of small trends in long-term datasets of variable quantities.

Finally, the two retrieval grids used in the Toronto and control analyses contained a similar number of layers and were constructed in a similar fashion, that is, with thin layers (~ 1 km) in the troposphere and gradually thickening layers in the stratosphere and above. Preliminary results of a further investigation of six other commonly employed retrieval grids containing 29–45 layers suggest that total column differences remain smaller than 1%. A detailed study of this implicit retrieval constraint is in progress.

4. Results

a. Ozone observations

Concentrations of ozone above Toronto were derived from 295 spectra recorded at SZAs between 25° and 65° in the NDACC filter 3 region (Table 1) between May 2002 and December 2004, since no continuous measurements are available for this time period in

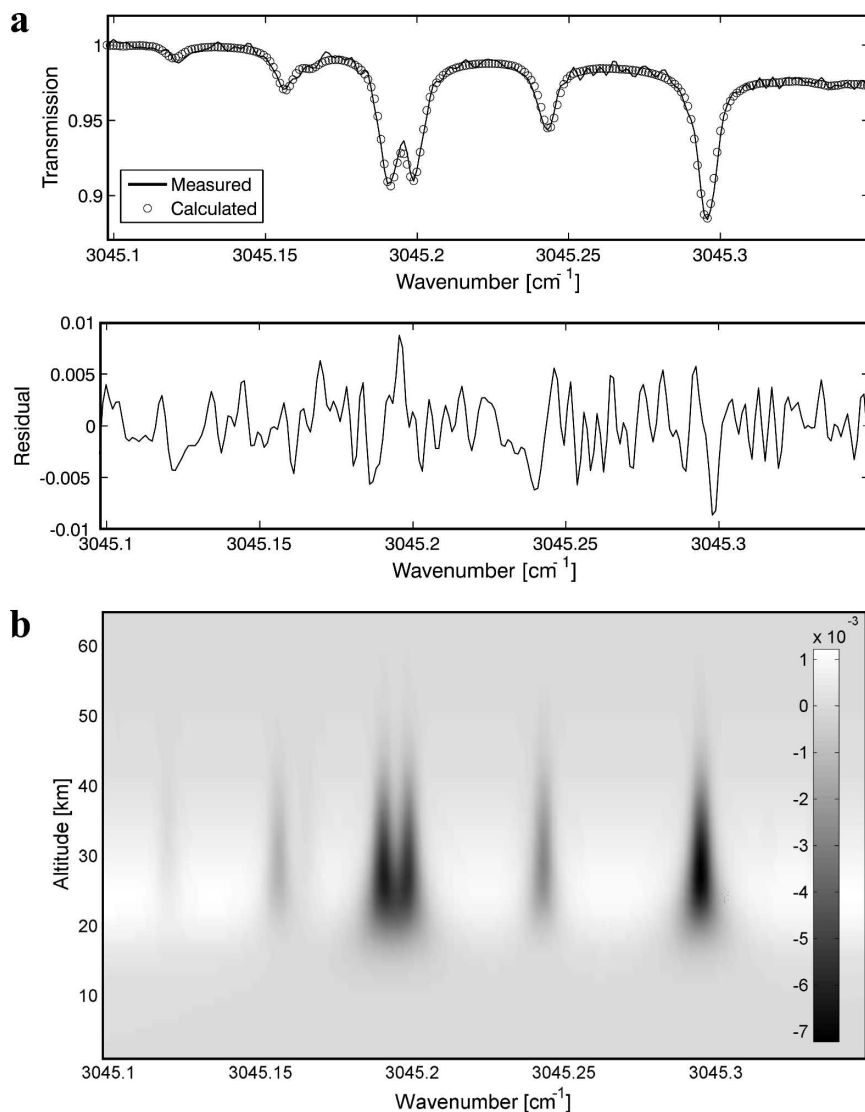


FIG. 8. (a) Typical spectral fit for ozone in the 3045 cm^{-1} microwindow. The residual has an RMS of 0.287% of the peak transmission in the microwindow. (b) Typical weighting function matrix (spectrum was recorded on 28 Aug 2003 at a solar zenith angle of 52.0°).

the filter 6 region used by, for example, Barret et al. (2002). Retrievals were carried out in the $3\nu_3$ band of ozone, in a microwindow spanning $3045.1\text{--}3045.35\text{ cm}^{-1}$ (Goldman et al. 1999; Mikhailenko et al. 2002; Griffith et al. 2003). The retrieval state vector has 44 elements: 38 for the vertical profile of ozone; 4 for the wavelength shift parameter, background slope, background curvature, and phase error; and 2 from scaling the vertical profiles of water vapor and methane, which interfere with the target gas in this microwindow.

The ozone a priori VMR profile was constructed from HALOE profiles (section 3b) between 15 and 60 km and the MIPAS reference profile outside of this altitude range. A priori profiles of pressure and tem-

perature were taken from NCEP for each day. Following the approach of Barret et al. (2002), the a priori covariance matrix for ozone was constructed to be diagonal with 20% variability at all of the 38 layers in the retrieval grid. The measurement error covariance matrix was also chosen to be diagonal and was constructed from the RMS SNR in the microwindow for each spectrum.

Figure 8a shows a representative microwindow spectral fit and its corresponding residual. Figure 8b shows the weighting function matrix that corresponds to this microwindow; the vertical sensitivity of the retrieval is plotted as a function of wavenumber and clearly correlated to the position and strength of ozone absorption

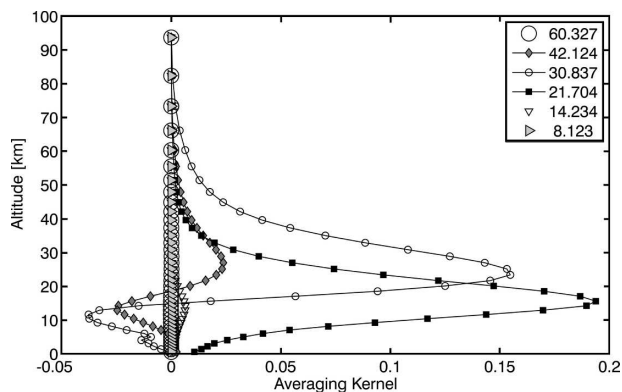


FIG. 9. Typical averaging kernels for the profile retrieval of ozone with their corresponding heights (km). This particular spectrum was recorded on 28 Aug 2003 at a solar zenith angle of 52.0°.

features in Fig. 8a. For each of the retrievals, the RMS value of the residuals (Fig. 8a) was used to judge the quality of the fits, with a quality assurance criterion set at 20% above the median. The median RMS value of the 2.5-yr time series was determined to be 0.284% of the peak transmission in the microwindow. The noise in the residuals is primarily random with small systematic features near the peak absorption of the ozone lines. Similar systematic structures have been observed by other groups performing fits in this microwindow (Griffith et al. 2003) with spectral parameters taken from the HITRAN database.

The vertical resolution of these ozone observations is characterized by the averaging kernel matrix [Eq. (4)]. Figure 9 shows the rows of the averaging kernels matrix

for a typical profile retrieval of ozone on the 38-layer height grid. The integrated area under each averaging kernel is a simple measure of the amount of non-a priori information that appears in the retrieval at the corresponding height (Rodgers 2000). It is clear that the retrieval is most sensitive in the stratosphere between 17 and 35 km, where the VMR of ozone peaks. The total column degrees of freedom for signal for ozone is approximately 2 (Table 3), and thus it is reasonable to report two independent partial columns in the stratosphere.

In a full information content analysis the transformed weighting function matrix is decomposed into its singular values and singular vectors (Fig. 10). [Rodgers (2000) shows that this is analytically equivalent to performing an eigenvalue decomposition on the square averaging kernel matrix.] The singular vectors that correspond to large singular values (approaching 1) represent spatial patterns in the true profile that are mapped to the row space of the measurement. The magnitudes of the singular values give an idea of the “sensitivity” of this mapping. The full width at half maximum (FWHM) of these leading-order singular vectors gives an idea of the vertical resolution in the measurement. Figure 10 shows the singular vectors that correspond to the six largest singular values and their corresponding degrees of freedom for signal for a measurement taken on 14 April 2004. The two degrees of freedom for signal in this ozone retrieval are almost entirely confined to the first three singular vectors, which qualitatively suggest a vertical resolution of approximately 10 km.

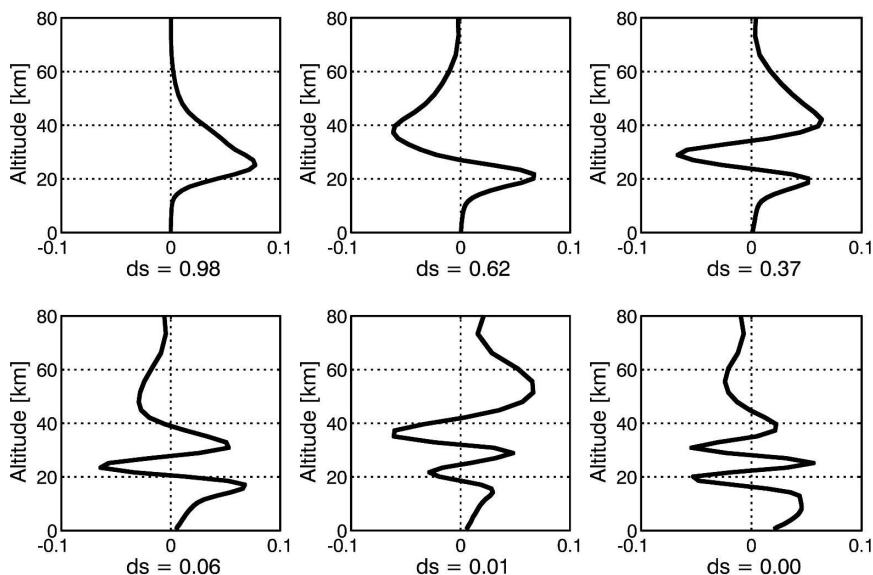


FIG. 10. Information content analysis: the six largest singular vectors of the transformed \mathbf{K} matrix with degrees of freedom for signal shown below each plot.

It is often convenient to construct partial columns that correspond to heights associated with the troposphere and the stratosphere as in Table 3; however, for comparison with satellite data the profile may need to be integrated to form different partial columns (section 4c).

b. Characterization of errors

By incorporating error terms into the formalism of the optimal estimation retrieval, Eq. (2) becomes

$$\hat{\mathbf{x}} = \mathbf{x}_a + \mathbf{A}(\mathbf{x} - \mathbf{x}_a) + \mathbf{G}\mathbf{K}_b(\mathbf{b} - \hat{\mathbf{b}}) + \mathbf{G}\Delta\mathbf{f} + \mathbf{G}\boldsymbol{\varepsilon}, \quad (7)$$

where the first two terms are part of the original formulation, the third term represents the error due to estimates of model parameters (\mathbf{b}) that are not retrieved, the fourth term is due to physical processes missing from the forward model, and the last term is known as the retrieval noise and represents the random error caused by measurement noise that propagates to the retrieval (Rodgers 1990). By taking the expectation value of the difference between the retrieved state and the true state, the following error covariance matrices are generated:

$$\begin{aligned} \mathbf{S}_s &= (\mathbf{A} - \mathbf{I})\mathbf{S}_x(\mathbf{A} - \mathbf{I})^T \\ \mathbf{S}_f &= \mathbf{G}\mathbf{K}_b\mathbf{S}_b\mathbf{K}_b^T\mathbf{G}^T \\ \mathbf{S}_{\varepsilon_x} &= \mathbf{G}\mathbf{S}_\varepsilon\mathbf{G}^T, \end{aligned} \quad (8)$$

where \mathbf{S}_s is the covariance of the error caused by smoothing of the true state by the averaging kernel, \mathbf{S}_f is the covariance of the error due to ill-described forward model parameters, $\mathbf{S}_{\varepsilon_x}$ is the covariance of the error due to random measurement error propagating to the retrieval, and \mathbf{I} is the identity matrix.

As the smoothing error is dependent on the true state of the atmosphere, it is calculated with a climatological covariance matrix, \mathbf{S}_x , which captures the natural variability of the atmosphere and which can differ from the \mathbf{S}_a matrix used in the retrievals. Typical smoothing error values for partial and total columns of seven trace gases retrieved at TAO are shown in Table 5, while typical measurement error values are shown in Table 6.

The model parameter error is dependent upon the covariance of the model parameters (\mathbf{b}), denoted by \mathbf{S}_b in Eq. (8). The primary model parameters that contribute to error in ozone retrievals are the temperature profiles, SZA, spectroscopic line parameters, and ILS (only ILS forward model parameters can be retrieved in the SFIT-2 OEM implementation). A detailed discussion of forward model errors for ozone is presented in Schneider et al. (2005a) who estimate errors at all

TABLE 5. Average smoothing error (%) in total and partial column retrievals in 2004.

	CH ₄	N ₂ O	O ₃	HCl	HF	NO	NO ₂
0–100 km	0.54	0.14	2.58	0.79	0.75	5.36	6.24
0–15 km	0.73	0.45	18.3	14.0	23.2	29.4	9.46
15–50 km	4.01	3.54	1.28	1.25	1.30	4.95	4.00

heights in the vertical profile retrieval due to the above quantities to be less than 4%, 1%, 5%, and 5%, respectively.

c. Intercomparison of a 2.5-yr time series of ozone

We show preliminary comparisons of ozone retrieved from spectra recorded at TAO with collocated measurements made by OSIRIS on the *Odin* satellite. Partial columns spanning 16–32 km were formed from TAO profile retrievals. Figure 11 shows strong overlap between the averaging kernels of the TAO total column and the stratospheric partial column, implying that the bulk of the total column is found between 16 and 32 km. As expected, neither kernel shows sensitivity to tropospheric ozone. Figure 12 shows the time series of daily stratospheric (16–32 km) column ozone measurements made by the TAO FTS between May 2002 and December 2004. The springtime ozone maximum can be seen in the data, which are more sparse during the fall and winter months due to cloudy conditions.

The OSIRIS instrument has been collecting ozone data from orbit since August 2001 (Llewellyn et al. 2004). The instrument measures vertical profiles of ozone by observing limb-scattered radiances between 280 and 800 nm. These vertical profiles are retrieved using a nonlinear Newtonian iteration version of optimal estimation (von Savigny et al. 2003) and span approximately 14–50 km, with a vertical resolution of 2 km. The coincidence criterion used for selecting spatially collocated measurements from the OSIRIS dataset (version 2.4) was $\pm 5^\circ$ in latitude and longitude. Figure 12 also shows the coincident daily OSIRIS stratospheric measurements (also between 16 and 32 km), which are sparse in fall months due to *Odin*'s focus on the Southern Hemisphere at that time. The qualita-

TABLE 6. Average measurement error (%) in total and partial column retrievals in 2004.

	CH ₄	N ₂ O	O ₃	HCl	HF	NO	NO ₂
0–100 km	0.80	0.28	1.83	0.97	1.00	2.87	2.28
0–15 km	0.84	0.36	4.21	6.38	11.7	2.59	0.73
15–50 km	1.62	1.81	1.78	0.73	0.77	4.22	5.88

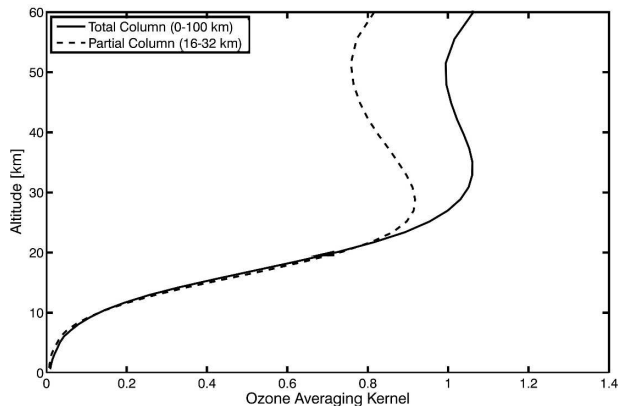


FIG. 11. Total and partial column averaging kernels for the retrieval of ozone concentrations from TAO-FTS spectra.

tive agreement between the TAO and OSIRIS datasets is good, with a few notable outliers in the summers of 2002 and 2004, and the winter/spring months in general. Disagreement between August and October 2004 is thought to be due to the small number of TAO measurements, which resulted from a problem with the heliostat at TAO that has since been resolved. Furthermore, due to the long horizontal pathlength characterizing OSIRIS observations, it is possible that some discrepancies are due to different air masses being sampled by the satellite instrument. For example, a pre-

liminary examination of potential vorticity (PV) maps has shown that a polar vortex filament has passed above Toronto in March 2004 when anomalous trace gas concentrations were recorded above the station; an investigation of the frequency of such events—which can lead to disagreements with satellite observations—is being conducted at TAO.

Petelina et al. (2005) showed that the OSIRIS ozone profiles are most reliable between 16 and 32 km in altitude and show the best agreement with other satellite instruments in this region. For this reason, the comparisons made here are restricted to this same region of the atmosphere, as previously noted. In comparing remote sensing measurements made by two instruments using different observation geometries, it is necessary to take into account the intrinsic differences between the averaging kernels of the two observing systems (Rodgers and Connor 2003). To this end, profiles observed by OSIRIS were smoothed with the TAO FTS averaging kernels as follows:

$$\mathbf{x}_{\text{smoothed}}^{\text{OSIRIS}} = \mathbf{A}^{\text{TAO}} \mathbf{x}^{\text{OSIRIS}} + (\mathbf{I} - \mathbf{A}^{\text{TAO}}) \times \mathbf{x}_a^{\text{TAO}}. \quad (9)$$

Since OSIRIS retrieves ozone concentrations with 2-km vertical resolution, it is appropriate to use Eq. (9) to smooth OSIRIS profiles to the much more coarse TAO resolution (~ 10 km). Finally, partial OSIRIS col-

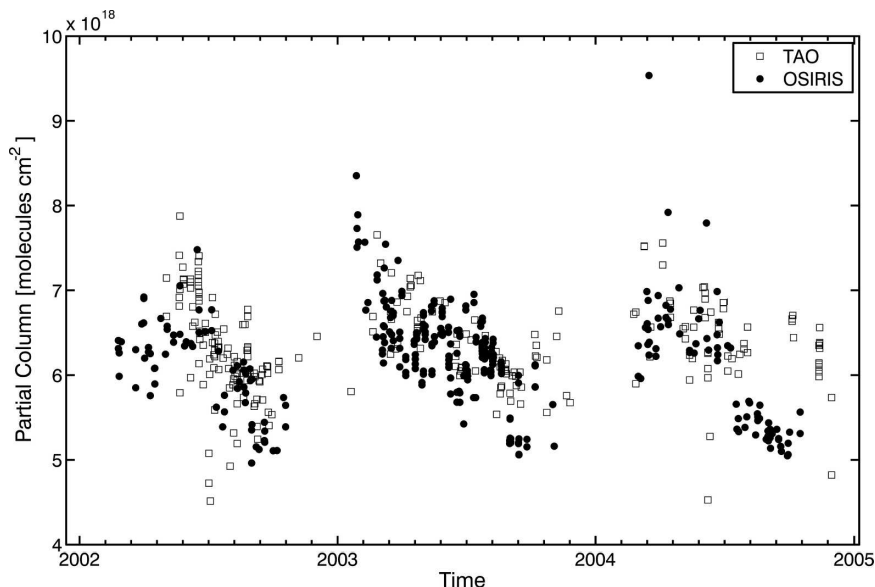


FIG. 12. Daily stratospheric ozone columns (16–32 km) recorded from May 2002 to December 2004 at TAO and by the OSIRIS satellite instrument within $\pm 5^\circ$ longitude and latitude of Toronto. The TAO error, calculated as the quadrature sum of smoothing and measurement errors [Eq. (8)] is on the order of 3%, while the OSIRIS (version 2.4) error has a median value of $\sim 5\%$.

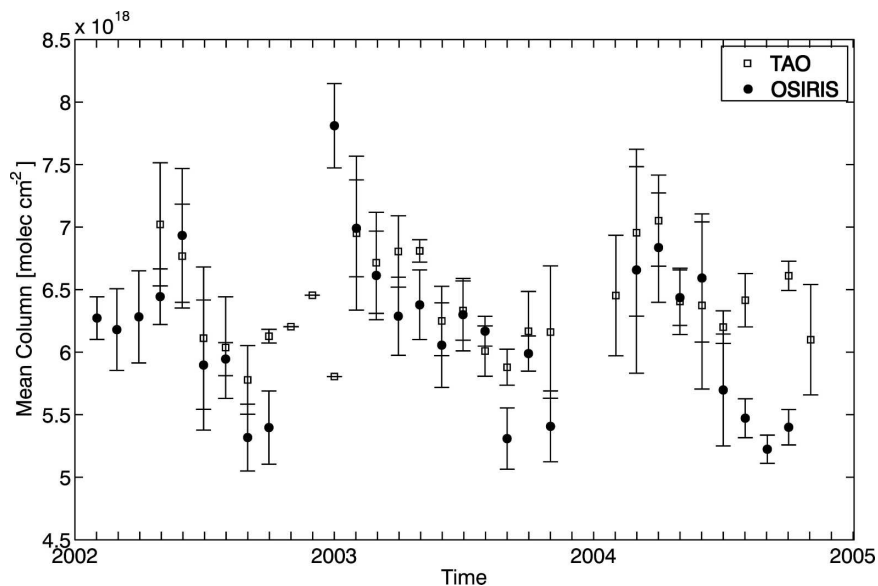


FIG. 13. Monthly mean stratospheric ozone column concentrations (16–32 km) observed at TAO and by OSIRIS. Error bars represent 1 std dev of the monthly means.

umns were derived by integrating the smoothed profiles.

To reduce the effect of temporal and spatial sampling inhomogeneities, monthly mean values were calculated from both datasets (Fig. 13). The agreement between monthly mean values in the stratosphere (16–32 km) is good for every month that TAO has been operational and where TAO and OSIRIS temporal coverage was high ($n > 5$). During the spring and summer months when the temporal coincidence is highest, almost all of the monthly means are in agreement with no consistent bias. Clear discrepancies exist for the winter months in which OSIRIS has limited viewing capability near Toronto and the increased presence of cloud cover severely limits the observing capabilities of the ground-based FTS. As a result, there are few measurements that span the October–February regions of any winter, potentially biasing the monthly means. For the months in which the TAO-FTS has only recorded one measurement (November 2002–January 2003), the error bars on the monthly means have been set to zero.

5. Conclusions

We have described the new optical design of a high-resolution Fourier transform infrared spectrometer, which serves as the primary instrument at the new Complementary Station of the NDACC in Toronto, Ontario, Canada. The ILS of the FTS has been quantified with the use of low-pressure HBr cell measurements and a previously described ILS parameter re-

trieval algorithm. We have outlined operational measurement settings used to record solar absorption infrared spectra at TAO since 2002. The OEM retrieval approach and its SFIT-2 algorithm implementation used to derive vertical profiles and partial columns of trace gases from TAO spectra were also reviewed. Some impacts of explicit and implicit retrieval constraints on retrieved total column amounts were described as part of the retrieval algorithm user intercomparison exercise performed by the TAO group in order to formally join the NDACC. During this exercise average differences between total columns retrieved from the same spectra by different users were below 2.1% for O_3 , 1.6% for HCl, and 0.3% for N_2O in the blind phase, and below 1% (0.83% for O_3 , 0.92% for HCl, and 0.05% for N_2O) in the open phase, when all retrieval constraints were identical.

The retrievals of O_3 , N_2O , CH_4 , HCl, HF, NO, and NO_2 have been characterized in terms of the number of independent pieces of information retrieved, and total and partial column smoothing and measurement errors, assuming an ideal instrument line shape function. The effect of the reduced modulation efficiency observed at maximum OPD on the information content of retrievals of trace gas profiles is the subject of current investigation, and efforts to optimize the FTS alignment are ongoing.

Finally, a 2.5-yr time series of the seven gases described above was submitted to the online NDACC archive (<http://www.ndsc.ws>) in 2005. The ozone retrievals were further characterized by their averaging

kernels, and a 2.5-yr time series of ozone partial columns (16–32 km) was compared to OSIRIS ozone partial columns from the same vertical region (smoothed by the TAO averaging kernels). The agreement between monthly means (when the number of TAO measurements is >5) is within 3% during this time interval, which is within the errors of both measurement platforms.

Acknowledgments. This work has been supported by NSERC, ABB Analytical Business PRU Québec, PREA, and CFCAS. TAO has been established with support from CFI, ORDCF, CRESTech, and the University of Toronto. We thank L. Boudreau, L. Rochette, C. Roy, and G. Baron of ABB Analytical Business PRU Québec for many useful interactions during instrument commissioning. We thank the OSIRIS team for providing ozone data (<http://osirus.usask.ca>). Finally, we thank all technicians, summer students, and postdoctoral fellows who contributed to measurements, lab support, and data analysis at TAO since 2000: C. Avis, P. Chen, B. Chugh, N. Faridi, C. Heald, K. MacQuarrie, O. Mikhailov, P. Rourke, R. Sullivan, D. Yashcov, and Y. Zhao.

REFERENCES

- Barret, B., M. De Mazière, and P. Demoulin, 2002: Retrieval and characterization of ozone profiles from solar infrared spectra at the Jungfraujoch. *J. Geophys. Res.*, **107**, 4788, doi:10.1029/2001JD001298.
- Bassford, M. R., C. A. McLinden, and K. Strong, 2001: Zenith-sky observations of stratospheric gases: The sensitivity of air mass factors to geophysical parameters and the influence of tropospheric clouds. *J. Quant. Spectrosc. Radiat. Transfer*, **68**, 657–677.
- , K. Strong, C. A. McLinden, and C. T. McElroy, 2005: Ground-based measurements of ozone and NO₂ during MANTRA 1998 using a new zenith-sky spectrometer. *Atmos.–Ocean*, **43**, 325–338.
- Bernardo, C., and D. W. T. Griffith, 2005: Fourier transform spectrometer instrument lineshape (ILS) retrieval by Fourier deconvolution. *J. Quant. Spectrosc. Radiat. Transfer*, **95**, 141–150.
- Carli, B., and Coauthors, 2004: First results of MIPAS/ENVISAT with operational level 2 code. *Adv. Space Res.*, **33**, 1012–1019.
- Coffey, M. T., A. Goldman, J. W. Hannigan, W. G. Mankin, W. G. Schoenfeld, C. P. Rinsland, C. Bernardo, and D. W. T. Griffith, 1998: Improved vibration-rotation (0-1) HBr line parameters for validating high resolution infrared atmospheric spectra measurements. *J. Quant. Spectrosc. Radiat. Transfer*, **60**, 863–867.
- Connor, B. J., N. B. Jones, S. W. Wood, J. G. Keys, C. P. Rinsland, and F. J. Murcray, 1996: Retrieval of HCl and HNO₃ profiles from ground-based FTIR data using SFIT2. *Proc. XVIII Quadrennial Ozone Symp.*, L'Aquila, Italy, International Ozone Commission, 485–488.
- Gallery, W. O., F. X. Kneizys, and S. A. Clough, 1983: Air mass computer program for atmospheric transmittance/radiance calculation: FSCATM. Environmental Research Paper ERP-828/AFGL-TR-83-0065, Air Force Geophysical Laboratory, Hanscom AFB, MA, 145 pp.
- Goldman, A., and Coauthors, 1999: Network for the Detection of Stratospheric Change Fourier transform infrared intercomparison at Table Mountain Facility, November 1996. *J. Geophys. Res.*, **104** (D23), 30 481–30 503.
- Goorvitch, D., 2000: Calculation of instrument functions. *J. Quant. Spectrosc. Radiat. Transfer*, **67**, 253–257.
- Griffith, D. W. T., N. B. Jones, B. McNamara, C. Paton Walsh, W. Bell, and C. Bernardo, 2003: Intercomparison of NDSC ground-based solar FTIR measurements of atmospheric gases at Lauder, New Zealand. *J. Atmos. Oceanic Technol.*, **20**, 1138–1153.
- Hase, F., T. Blumenstock, and C. Paton-Walsh, 1999: Analysis of the instrumental line shape of high-resolution Fourier transform IR spectrometers with gas cell measurements and new retrieval software. *Appl. Opt.*, **38**, 3417–3422.
- , J. W. Hannigan, M. T. Coffey, A. Goldman, M. Höpfner, N. B. Jones, C. P. Rinsland, and S. W. Wood, 2004: Intercomparison of retrieval codes used for the analysis of high-resolution, ground-based FTIR measurements. *J. Quant. Spectrosc. Radiat. Transfer*, **87**, 25–52.
- Kurylo, M. J., and R. J. Zander, 2000: The NDSC—Its status after ten years of operation. *Proc. 19th Quadrennial Ozone Symp.*, Sapporo, Japan, Hokkaido University, 167–168.
- Llewellyn, E. J., and Coauthors, 2004: The OSIRIS instrument on the Odin spacecraft. *Can. J. Phys.*, **82**, 411–422.
- McElroy, C. T., 1995: A spectroradiometer for the measurement of direct and scattered solar irradiance from on-board the NASA ER-2 high-altitude research aircraft. *Geophys. Res. Lett.*, **22**, 1361–1364.
- Meier, A., A. Goldman, P. S. Manning, T. M. Stephen, C. P. Rinsland, N. B. Jones, and S. W. Wood, 2004: Improvements to air mass calculations for ground-based infrared measurements. *J. Quant. Spectrosc. Radiat. Transfer*, **83**, 109–113.
- , and Coauthors, 2005: Evidence of reduced measurement uncertainties from an FTIR instrument intercomparison at Kiruna, Sweden. *J. Quant. Spectrosc. Radiat. Transfer*, **96**, 75–84.
- Mikhailenko, S., A. Barbe, and V. L. G. Tyuterev, 2002: Extended analysis of line positions and intensities of ozone bands in the 2900–3400 cm⁻¹ region. *J. Mol. Spectrosc.*, **215**, 29–41.
- Murtagh, D., and Coauthors, 2002: An overview of the Odin atmospheric mission. *Can. J. Phys.*, **80**, 309–318.
- Park, J. H., 1982: Effect of interferogram smearing on atmospheric limb sounding by Fourier transform spectroscopy. *Appl. Opt.*, **21**, 1356–1366.
- Paton Walsh, C., and Coauthors, 1997: An uncertainty budget for ground-based Fourier transform infrared column measurements of HCl, HF, N₂O, and HNO₃ deduced from results of side-by-side instrument intercomparisons. *J. Geophys. Res.*, **102** (D7), 8867–8873.
- Petelina, S. V., and Coauthors, 2005: Validation of ACE-FTS stratospheric ozone profiles against Odin/OSIRIS measurements. *Geophys. Res. Lett.*, **32**, L15S06, doi:10.1029/2005GL022377.
- Pougatchev, N. S., B. J. Connor, and C. P. Rinsland, 1995: Infrared measurements of the ozone vertical distribution above Kitt Peak. *J. Geophys. Res.*, **100** (D8), 16 689–16 697.
- Rinsland, C. P., and Coauthors, 1998: Northern and Southern Hemisphere ground-based infrared spectroscopic measure-

- ments of tropospheric carbon monoxide and methane. *J. Geophys. Res.*, **103** (D21), 28 197–28 217.
- , A. Meier, D. W. T. Griffith, and L. S. Chiou, 2001: Ground-based measurements of tropospheric CO, C₂H₆, and HCN from Australia at 34°S latitude during 1997–1998. *J. Geophys. Res.*, **106** (D18), 20 913–20 924.
- , and Coauthors, 2002a: Multiyear infrared solar spectroscopic measurements of HCN, CO, C₂H₆, and C₂H₂ tropospheric columns above Lauder, New Zealand (45°S latitude). *J. Geophys. Res.*, **107**, 4185, doi:10.1029/2001JD001150.
- , and Coauthors, 2002b: Ground-based infrared spectroscopic measurements of carbonyl sulfide: Free tropospheric trends from a 24-year time series of solar absorption measurements. *J. Geophys. Res.*, **107**, 4657, doi:10.1029/2002JD002522.
- , and Coauthors, 2003: Long-term trends of inorganic chlorine from ground-based infrared solar spectra: Past increases and evidence for stabilization. *J. Geophys. Res.*, **108**, 4252, doi:10.1029/2002JD003001.
- Rodgers, C. D., 1976: Retrieval of atmospheric temperature and composition from remote measurements of thermal radiation. *Rev. Geophys. Space Phys.*, **14**, 609–624.
- , 1990: Characterization and error analysis of profiles retrieved from remote sounding measurements. *J. Geophys. Res.*, **95** (D5), 5587–5595.
- , 2000: *Inverse Methods For Atmospheric Sounding: Theory and Practice*. World Scientific, 238 pp.
- , and B. J. Connor, 2003: Intercomparison of remote sounding instruments. *J. Geophys. Res.*, **108**, 4116, doi:10.1029/2002JD002299.
- Rothman, L. S., and Coauthors, 2003: The HITRAN molecular spectroscopic database: Edition of 2000 including updates through 2001. *J. Quant. Spectrosc. Radiat. Transfer*, **82**, 5–44.
- , and Coauthors, 2005: The HITRAN 2004 molecular spectroscopic database. *J. Quant. Spectrosc. Radiat. Transfer*, **96**, 139–204.
- Russell, J. M., III, and Coauthors, 1993: The Halogen Occultation Experiment. *J. Geophys. Res.*, **98** (D6), 10 777–10 797.
- Schneider, M., T. Blumenstock, F. Hase, M. Höpfner, E. Cuevas, A. Redondas, and J. M. Sancho, 2005a: Ozone profiles and total column amounts derived at Izaña, Tenerife Island, from FTIR solar absorption spectra, and its validation by an intercomparison to ECC-sonde and Brewer spectrometer measurements. *J. Quant. Spectrosc. Radiat. Transfer*, **91**, 245–274.
- , and Coauthors, 2005b: Subtropical trace gas profiles determined by ground-based FTIR spectroscopy at Izaña (28° N, 16° W): Five-year record, error analysis, and comparison with 3-D CTMs. *Atmos. Chem. Phys.*, **5**, 153–167.
- von Savigny, C., and Coauthors, 2003: Stratospheric ozone profiles retrieved from limb scattered sunlight radiance spectra measured by the OSIRIS instrument on the Odin satellite. *Geophys. Res. Lett.*, **30**, 1755, doi:10.1029/2002GL016401.
- Zander, R., and Coauthors, 1994: Secular trend and seasonal variability of the column abundance of N₂O above the Jungfraujoch station determined from IR solar spectra. *J. Geophys. Res.*, **99** (D8), 16 745–16 756.